Tuneable elastomeric nanochannels for nanofluidic manipulation

DONGEUN HUH[1], K. L. MILLS[2], XIAOYUE ZHU[1], MARK A. BURNS[1,3], M. D. THOULESS[2] AND SHUICHI TAKAYAMA[1,4]*

[1]Department of Biomedical Engineering, University of Michigan, 2200 Bonisteel Blvd, Ann Arbor, Michigan 48109-2099, USA
[2]Department of Mechanical Engineering, University of Michigan, 2350 Hayward St., Ann Arbor, Michigan 48109-2125, USA
[3]Department of Chemical Engineering, University of Michigan, 2300 Hayward St., Ann Arbor, Michigan 48109-2136, USA
[4]Macromolecular Science and Engineering Center, University of Michigan, 2300 Hayward St., Ann Arbor, Michigan 48109, USA
*e-mail: takayama@umich.edu

Published online: 7 May 2007; corrected online 9 May 2007 (details online); doi:10.1038/nmat1907

Fluidic transport through nanochannels offers new opportunities to probe fundamental nanoscale transport phenomena[1–5] and to develop tools for manipulating DNA[6–16], proteins[17,18], small molecules[19,20] and nanoparticles[21,22]. The small size of nanofabricated devices and the accompanying increase in the effect of surface forces[23,24], however, pose challenges in designing and fabricating flexible nanofluidic systems that can dynamically adjust their transport characteristics according to the handling needs of various molecules and nanoparticles. Here, we describe the use of nanoscale fracturing of oxidized poly(dimethylsiloxane) to conveniently fabricate nanofluidic systems with arrays of nanochannels that can actively manipulate nanofluidic transport through dynamic modulation of the channel cross-section. We present the design parameters for engineering material properties and channel geometry to achieve reversible nanochannel deformation using remarkably small forces. We demonstrate the versatility of the elastomeric nanochannels through tuneable sieving and trapping of nanoparticles, dynamic manipulation of the conformation of single DNA molecules and *in situ* photofabrication of movable polymeric nanostructures.

The nanofluidic system consists of a parallel array of nanochannels made in poly(dimethylsiloxane) (PDMS). Fluid flows are driven mainly by an electric field applied between the inlet and outlet compartments (Fig. 1a,b). The channel geometry and materials mechanics are optimized so that the cross-sectional size of the nanochannels can be reversibly modulated in response to compressive forces applied perpendicularly to the nanochannels. As the nanochannels only allow the passage of molecules or nanoparticles that are smaller than their cross-section (see the Supplementary Information), the magnitude of applied force can be varied to choose subpopulations in a polydisperse mixture that can pass through the nanochannels. For example, the size of non-deformed nanochannels supports co-transport of larger and smaller particles (Fig. 1c). Moderate channel deformation at low levels of applied force, however, hinders larger particles from entering the nanochannels and allows selective transport of the smaller particles (Fig. 1d). A further increase in the applied force causes the nanochannels to close, excluding sample particles (Fig. 1e). This adjustability permits manifold modes of nanofluidic transport within a single device for a given sample population. Channel deformation can also be used to trap nanoparticles already inside the nanochannels by mechanically constraining their movement. When the applied force is removed, recovery of flow prompts trapped nanoparticles to resume their movement along the nanochannels (Fig. 1f).

Fabrication of the elastomeric nanochannels begins with mechanical stretching of plasma-oxidized PDMS to generate an ordered array of nanoscale cracks[25,26], which are replicated onto ultraviolet-curable epoxy (see Fig. 2a and Supplementary Information). A substrate with recessed nanochannels is prepared by casting PDMS prepolymer against the epoxy master. We adjusted the production parameters of crack patterning to create pre-sealed nanochannels having the shape of an isosceles triangle with a base length of 688 ± 79 nm (mean $\pm$ s.d.) and a height of 78 ± 18 nm. Finally, the PDMS substrate is oxidized and brought into conformal contact with a flat slab of oxidized PDMS to yield an array of tightly sealed nanochannels (see Fig. 2b and Supplementary Information).

The crucial steps for ensuring complete sealing and reversible functionality of nanochannels are (1) a brief (30–60 s) oxidation of the PDMS before the bonding, (2) the use of the epoxy master and (3) the use of a relatively stiff PDMS to prevent irreversible channel collapse (see the Supplementary Information)[27–29]. A thin oxidized layer is necessary to ensure adequate surface compliance for sealing. For cracking, however, a thick oxidation layer was necessary to induce the requisite crack characteristics. Hence, an epoxy master was used in the intermediate step so that each of these conditions could be satisfied.

Nanochannels formed by cracking have a triangular cross-section in which channel closure proceeds gradually from the corners. This is in contrast to rectangular channels that close by a sudden yet partial collapse at the middle[23]. Dimensional analysis shows that the extent of channel closure, c_c, is given by

$$\frac{c_c}{a} = f\left(\frac{a}{h}, \frac{h_f}{h}, \frac{\bar{E}_2 h^2}{\gamma a}, \frac{\sigma_a}{\bar{E}_2}, \frac{\bar{E}_1}{\bar{E}_2}\right),$$

where $\bar{E}_1$ and $\bar{E}_2$ are the plane-strain moduli of the oxidized layer and PDMS, respectively; γ is the surface energy of the nanochannels; σ_a is the remote applied compressive stress; h and $2a$ are the height and base length of the cross-section, respectively; h_f is the thickness of the oxidized layer

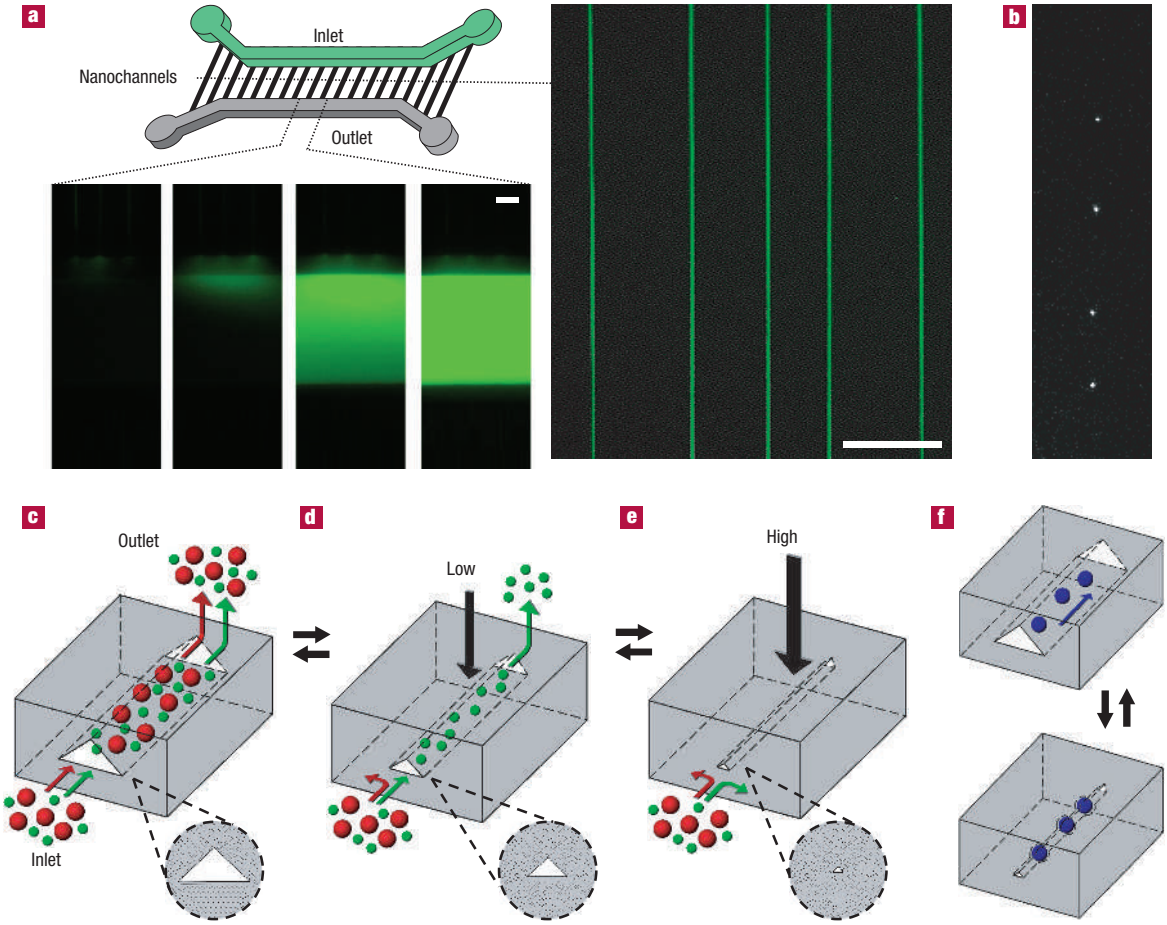

Figure 1 Size-adjustable elastomeric nanochannels. a, The system has an array of nanochannels spanning microscale inlet and outlet compartments separated by 500 μm. Fluorescein molecules introduced into the inlet are transported through the nanochannels by electrokinetic flows driven at ~62 V cm^{-1} (right inset). The four bottom insets show fluorescence intensity in the outlet at time = 0, 4, 16 and 24 s, respectively (from left to right). Scale bars: 20 μm. **b**, A single-file flow of single 20 nm quantum dots along a nanochannel. **c**, The larger cross-section of relaxed nanochannels allows both larger and smaller particles to pass through simultaneously. **d**, Elastomeric nanochannels are compressed to change their cross-sectional size. Low levels of compressive stress (22 kPa) constrict the channel such that the larger particles are prevented from entering the nanochannels, and only the smaller particles pass through. **e**, Nanochannels loaded with larger stresses (42 kPa) become extremely small, excluding sample particles regardless of their size. The mode of transport with different size-selectivity can be switched reversibly by changing the magnitude of applied force. **f**, Channel deformation traps single nanoparticles. The particles are released and resume their motion on removal of applied force.

(Fig. 2c). To determine the normalized closure distance, c_c/a, as a function of $\bar{E}_2h^2/\gamma a$, $\bar{E}_1/\bar{E}_2$ and $\sigma_a/\bar{E}_2$, we carried out finite-element simulations (see the Supplementary Information) using a fixed initial geometry consistent with the experimental configuration ($a/h = 5$, $h_f/h = 1.7$). We found that for a given material, there is a critical value of $\bar{E}_2h^2/\gamma a$ above which nanochannels can be supported without spontaneous collapse. When non-oxidized PDMS is used ($\bar{E}_1/\bar{E}_2 = 1$), $\bar{E}_2h^2/\gamma a$ of our system (~1.5) lies well below its critical value (~10), causing the nanochannels to collapse spontaneously (see Fig. 2d and Supplementary Information, Fig. S3). An effective way to reduce the critical value without increasing the modulus of the bulk PDMS and hence without sacrificing size-adjustability is to generate a thin layer of stiff material immediately in the vicinity of the nanochannel. A brief oxidation accomplishes this by raising $\bar{E}_1/\bar{E}_2$ to roughly 130, in which case the critical $\bar{E}_2h^2/\gamma a$ becomes smaller by an order of magnitude and the channels remain open (see Fig. 2d and Supplementary Information, Fig. S3). Under this condition, the compliance of PDMS permits reversible closure of the nanochannels using compression. We optimized the fabrication parameters to achieve a fine balance between the geometry, elastic properties and surface forces, which allows $\bar{E}_2h^2/\gamma a$ of the system to be above yet close to its critical value. In this range, the cross-sectional size changes dramatically in response to a compressive force, enabling the manipulation of channel closure using very small stresses (Fig. 2e).

We demonstrated sieving of molecules and nanoparticles with tuneable size-selectivity using a suspension containing red-fluorescent sulphorhodamine (SR)-101 molecules and 35 nm green-fluorescent quantum dots (Fig. 3a) (see the Supplementary Information for electrical resistance measurements and electrokinetic transport of single molecular species across the nanochannels). Fluorescence-intensity measurements at the outlet showed that the larger cross-section of non-deformed nanochannels permitted co-transport of SR and quantum dots (Fig. 3b). When the nanochannels were compressed with 22 kPa of pressure (see the Supplementary Information), green fluorescence was not detected, whereas the red fluorescence still increased,

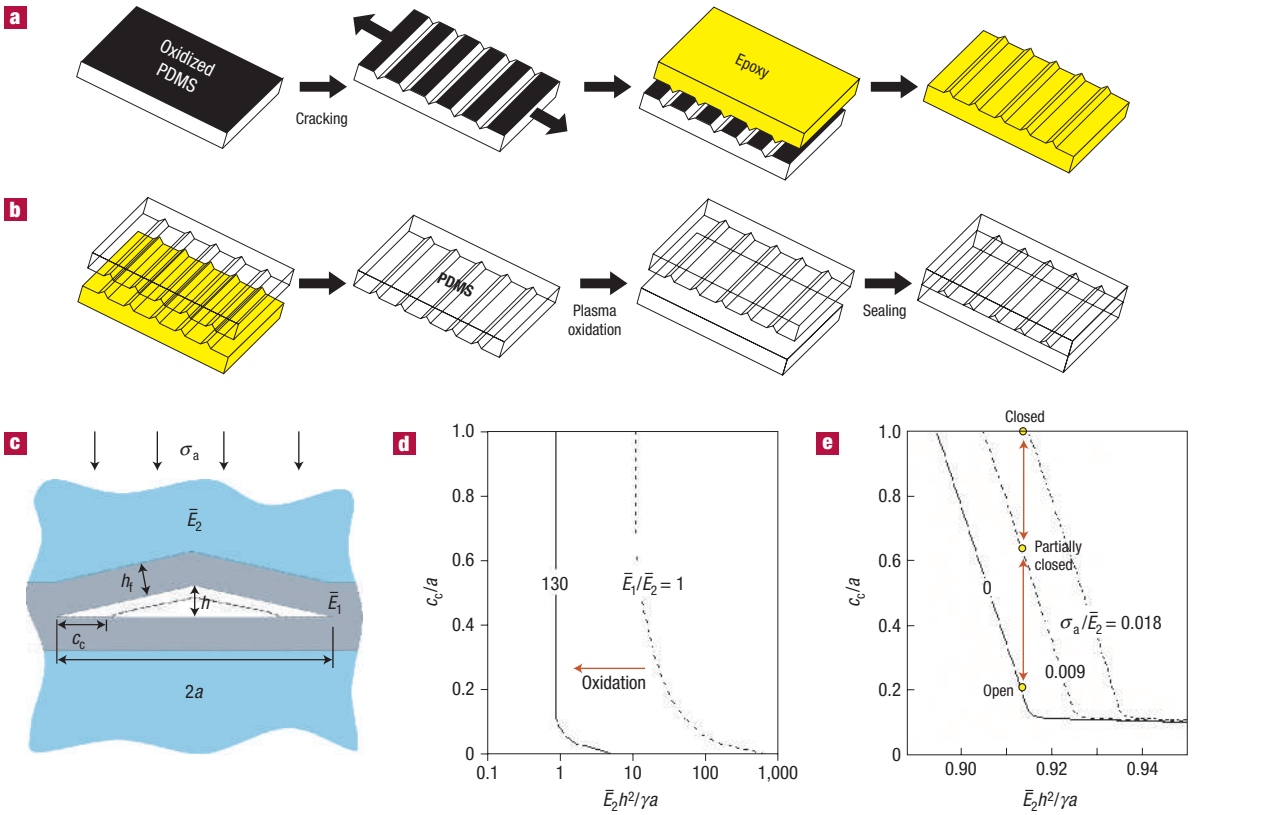

Figure 2 Fabrication of structurally stable elastomeric nanochannels. a, A PDMS slab exposed to oxygen plasma is stretched to generate linear nanoscale cracks. The nanocracks are replicated onto ultraviolet-curable epoxy. **b**, PDMS prepolymer is cast against the epoxy mould to generate negative relief patterns of nanochannels. The PDMS substrate is then briefly oxidized and sealed against an oxidized PDMS slab to form an array of enclosed nanochannels. **c**, The cross-section of relaxed nanochannels can be approximated as an isosceles triangle with an average base length of 688 nm ($2a$) and an average height of 78 nm (h). **d**, Normalized closure distance (c_c/a) plotted against $\bar{E}_2h^2/\gamma a$ for both the non-oxidized ($\bar{E}_1/\bar{E}_2 = 1$) and oxidized ($\bar{E}_1/\bar{E}_2 = 130$) states when there is no applied compressive stress ($\sigma_a/\bar{E}_2 = 0$). **e**, The solid and dashed lines indicate the closure distance for relaxed and compressed nanochannels, respectively. Note that $\bar{E}_1/\bar{E}_2 = 130$. Reversible closure of the nanochannels is demonstrated by the reversible vertical jumps to and from the dashed lines (shown with red arrows) when remote stresses are applied or removed, respectively ($\sigma_a/\bar{E}_2 = 0.018$ and 0.009, corresponding to $\sigma_a = 22$ and 42 kPa, respectively).

although at a much slower rate (Fig. 3c). This indicates that the decrease in the channel cross-sectional area completely obstructed the flow of the larger quantum dots while partially impeding the transport of SR. Application of the compressive stress of 42 kPa resulted in closed channels and hence no detectable fluorescence (Fig. 3d). In all cases, the difference in fluorescence intensity between the observation area and other regions of the outlet was less than 5%, suggesting fairly uniform transport throughout an array of nanochannels. These results show that even for the same particle population, this system is capable of generating multiple configurations of molecular or nanoparticle transport that can be switched dynamically.

Controlled channel constriction can also trap and release single nanoparticles. Without compressive force, a quantum dot (diameter ~ 20 nm) moves unidirectionally along the length of the nanochannels (Fig. 3e). The velocities of moving nanoparticles in different channels were measured to be uniform across the array with a channel-to-channel variation of approximately 4.3%. When deformed by 42 kPa of applied pressure, however, the nanochannels trap the particle securely by causing it to halt and remain stationary without brownian motion (Fig. 3f). Subsequent removal of applied force allows the trapped quantum dot to continue its motion down the channel (Fig. 3g). This method offers a simple means to manipulate the movement of particles at the nanoscale without using their electrical or chemical properties. Moreover, the channel adjustability may allow more robust nanofluidic manipulation over a wider range of nanoparticle sizes.

The elastomeric nanochannels can also confine and dynamically manipulate single DNA molecules. When electrophoretically driven into nanochannels, fluorescently labelled λ-phage DNA (48.5 kbp) was stretched to ~5.6 μm (see the Supplementary Information), which is approximately 30% of its fully stretched length[12]. Once partially stretched, the DNA molecules travelled down the nanochannels in an electrophoretic fashion without any significant change in their length (Fig. 4a). When the channel size was reduced by applying 22 kPa of pressure, however, the migration was initially replaced by further elongation of the DNA presumably owing to the reduction in entropy[12]. Further stretching was achieved by selective electrophoretic movement of the downstream end with little movement of the upstream end (Fig. 4b). The DNA continued its extension until it reached an equilibrium length of ~13.6 μm, after which time the entire length of the molecule resumed its uniform electrophoretic motion. When the compressive force was removed, the stretched DNA strand shrank to its original extended length in less than 1 min as a result of entropic relaxation in the non-deformed nanochannel

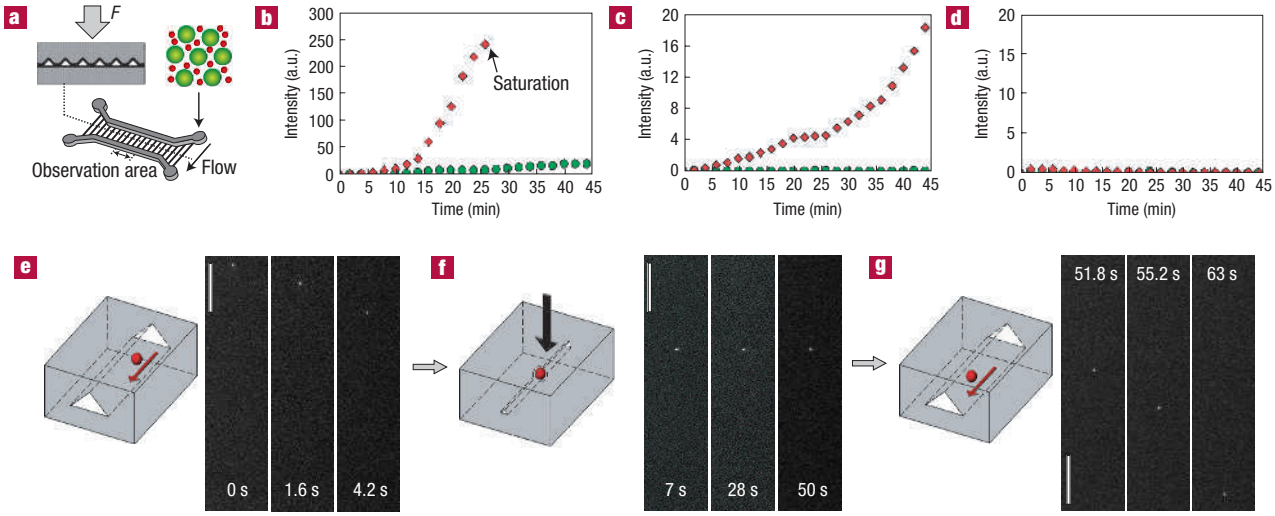

Figure 3 Nanofluidic sample trafficking using tuneable size-selectivity and single-nanoparticle trapping. a, SR-101 molecules (molecular mass ~ 607 daltons) and 35 nm quantum dots were introduced into the inlet. Electrokinetic transport through water-filled nanochannels was quantified by fluorescence detection in the observation area. Flows were driven by ~ 69 V cm^{-1}. **b**, Without force, both green and red fluorescence increase as a result of co-transport of SR (red diamond) and quantum dots (green circle). The smaller size of SR leads to a higher rate of intensity increase (a.u. = arbitrary unit). **c**, Channel deformation by 22 kPa prohibits the transport of quantum dots and retards the movement of SR (slower increase in red fluorescence). **d**, When compressed with 42 kPa, the nanochannels hinder the transport of both species, as shown by the lack of measurable increase in fluorescence. **e**, A single 20 nm quantum dot travelling along a relaxed nanochannel. Quantum dots were suspended in an aqueous bovine serum albumin solution (10 mg ml^{-1}). **f**, Channel deformation at 42 kPa traps the particle. **g**, Release of applied force resumes the flow of carrier liquid and the motion of the quantum dot. Scale bars: 16 μm.

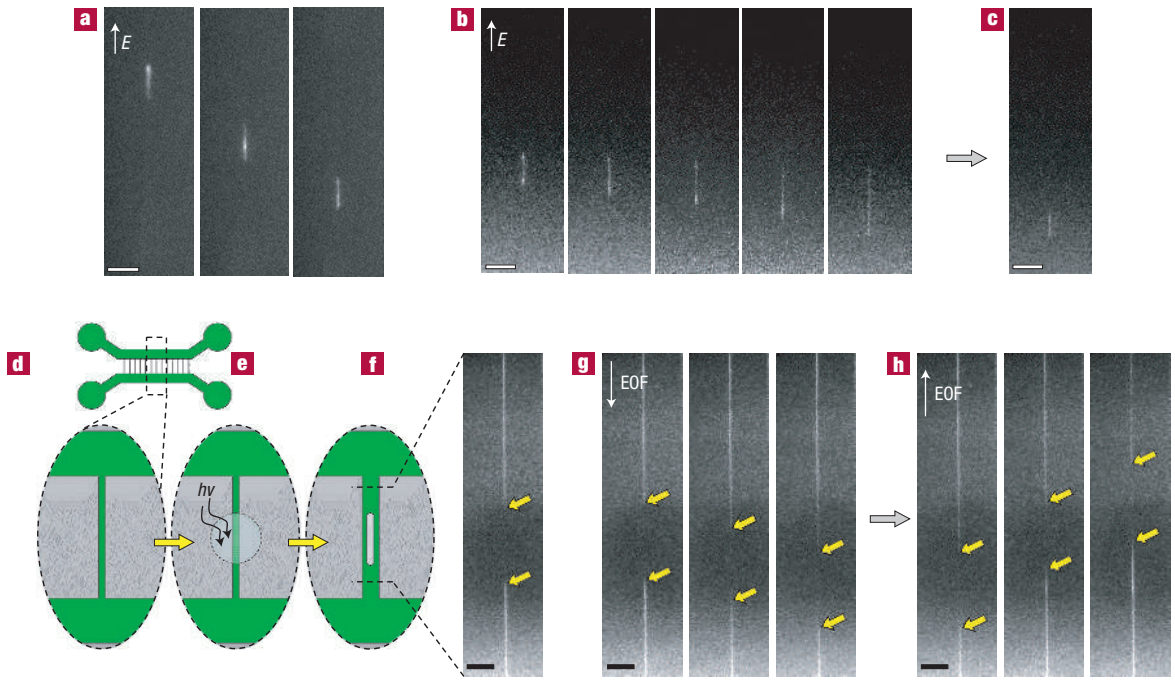

Figure 4 DNA manipulation and *in situ* fabrication of movable nanostructures. a, Electrophoretic migration of a partially extended 48.5-kbp-long λ-phage DNA in a relaxed nanochannel by 34.5 V cm^{-1} (time interval between frames = 0.8 s). *E* represents electric field. **b**, Channel deformation at 22 kPa resulted in further stretching of the DNA to 13.6 μm at the same electric field (time interval between frames = 0.6 s). **c**, Removal of compression after the electric field was switched off caused the DNA molecule to relax to its original length. Scale bars: 5 μm. For in-channel photofabrication, a solution containing acrylamide monomers, photoinitiator and fluorescein is introduced into the nanochannels. **d**, The nanochannels are constricted by the compressive stress of 22 kPa. **e**, A target area is selectively polymerized by ultraviolet. Subsequently, strong illumination photobleaches the polymerized region. **f**, Restoration of the channel size releases the polyacrylamide nanofilament. In fluorescence imaging, the filament appeared as a dark segment. Yellow arrows represent the extremities of the filament. **g**, The nanofilament can be manipulated to move along the nanochannel by electro-osmotic flow (EOF). **h**, The motion is reversed when the direction of electro-osmotic flow changes. Scale bars: 10 μm.

(Fig. 4c). The ability to modulate entropy dynamically and reversibly opens new possibilities to investigate and manipulate dynamic behaviours of DNA and other biopolymers at the single-molecule level.

Finally, we expanded the operation of this system to in-channel photopolymerization of filamentous polyacrylamide nanostructures that can be actuated to move through the nanochannels. Relaxed nanochannels are filled with acrylamide/bisacrylamide monomer solution mixed with photoinitiator and fluorescein (see the Supplementary Information). The nanochannel cross-section is then reduced using 22 kPa of applied stress (Fig. 4d), and ultraviolet light is irradiated onto a small area spanning ~25 μm along the channel length for 5 min to induce localized photopolymerization (Fig. 4e). Subsequently, fluorescein in the exact same region is selectively photobleached by strong illumination to facilitate imaging of the polymerized gel. Finally, by removing the compression, the nanochannel recovers its original size, creating a polymerized polyacrylamide nanofilament 'floating' inside the nanochannel (Fig. 4f). Electro-osmotic flows cause the nanofilaments to slide along the nanochannels, and the direction of the movement can be manipulated by switching the polarity of the electric field (Fig. 4g,h). This approach provides unique capabilities to fabricate nanoscale moving parts whose minimum feature size is limited only by the size of the nanochannels, offering advantages over conventional photolithography or hydrogel-based fabrication platforms[30].

The nanochannels described here are straightforward to fabricate and provide a remarkably versatile example of an active nanostructure that can change its architecture during operation to create, control and manipulate various types of nanofluidic transport. Designing these adjustable elastomeric structures requires not only the reduction in feature sizes, but more importantly the engineering of the channel surface and the deformability of elastomers to accommodate the contradicting need for structural stability and adjustability. We believe that this approach can be extended to higher levels of functionality through the integration of parallel and serial operations, sophisticated optics and a wealth of polymer chemistry.

Received 9 January 2007; accepted 4 April 2007; published 7 May 2007.

References

1. Chen, J. Y., Kutana, A., Collier, C. P. & Giapis, K. P. Electrowetting in carbon nanotubes. *Science* **310**, 1480–1483 (2005).
2. Pennathur, S. & Santiago, J. G. Electrokinetic transport in nanochannels. 2. Experiments. *Anal. Chem.* **77**, 6782–6789 (2005).
3. Pu, Q., Yun, J., Temkin, H. & Liu, S. Ion-enrichment and ion-depletion effect of nanochannel structures. *Nano Lett.* **4**, 1099–1103 (2004).
4. Eijkel, J. C. T., Bomer, J. G. & van den Berg, A. Osmosis and pervaporation in polyimide submicron microfluidic channel structures. *Appl. Phys. Lett.* **87**, 114103 (2005).
5. Garcia, A. L. *et al.* Electrokinetic molecular separation in nanoscale fluidic channels. *Lab Chip* **5**, 1271–1276 (2005).
6. Han, J. & Craighead, H. G. Separation of long DNA molecules in a microfabricated entropic trap array. *Science* **288**, 1026–1029 (2000).
7. Reccius, C. H., Mannion, J. T., Cross, J. D. & Craighead, H. G. Compression and free expansion of single DNA molecules in nanochannels. *Phys. Rev. Lett.* **95**, 268101 (2005).
8. Tegenfeldt, J. O. *et al.* The dynamics of genomic-length DNA molecules in 100-nm channels. *Proc. Natl Acad. Sci. USA* **101**, 10979–10983 (2004).
9. Guo, L. J., Cheng, X. & Chou, C.-F. Fabrication of size-controllable nanofluidic channels by nanoimprinting and its application for DNA stretching. *Nano Lett.* **4**, 69–73 (2004).
10. Foquet, M., Korlach, J., Zipfel, W., Webb, W. W. & Craighead, H. G. DNA fragment sizing by single molecule detection in submicrometer-sized closed fluidic channels. *Anal. Chem.* **74**, 1415–1422 (2002).
11. Campbell, L. C., Wilkinson, M. J., Manz, A., Camilleri, P. & Humphreys, C. J. Electrophoretic manipulation of single DNA molecules in nanofabricated capillaries. *Lab Chip* **4**, 225–229 (2004).
12. Reisner, W. *et al.* Statics and dynamics of single DNA molecules confined in nanochannels. *Phys. Rev. Lett.* **94**, 196101 (2005).
13. Fu, J. P., Schoch, R. B., Stevens, A. L., Tannenbaum, S. R. & Han, J. Y. A patterned anisotropic nanofluidic sieving structure for continuous-flow separation of DNA and proteins. *Nature Nanotech.* **2**, 121–128 (2007).
14. Craighead, H. G. Future lab-on-a-chip technologies for interrogating individual molecules. *Nature* **442**, 387–393 (2006).
15. Riehn, R., Austin, R. H. & Sturm, J. C. A nanofluidic railroad switch for DNA. *Nano Lett.* **6**, 1973–1976 (2006).
16. Riehn, R. *et al.* Restriction mapping in nanofluidic devices. *Proc. Natl Acad. Sci. USA* **102**, 10012–10016 (2005).
17. Wang, Y.-C., Stevens, A. L. & Han, J. Million-fold preconcentration of proteins and peptides by nanofluidic filter. *Anal. Chem.* **77**, 4293–4299 (2005).
18. Sivanesan, P., Okamoto, K., English, D., Lee, C. S. & DeVoe, D. L. Polymer nanochannels fabricated by thermomechanical deformation for single-molecule analysis. *Anal. Chem.* **77**, 2252–2258 (2005).
19. Jirage, K. B., Hulteen, J. C. & Martin, C. R. Nanotubule-based molecular filtration membranes. *Science* **278**, 655–658 (1997).
20. Lee, S. B. *et al.* Antibody-based bio-nanotube membranes for enantiomeric drug separations. *Science* **296**, 2198–2200 (2002).
21. Stavis, S. M., Edel, J. B., Samiee, K. T. & Craighead, H. G. Single molecule studies of quantum dot conjugates in a submicrometer fluidic channel. *Lab Chip* **5**, 337–343 (2005).
22. Drazer, G., Koplik, J. & Acrivos, A. Absorption phenomena in the transport of a colloidal particle through a nanochannel containing a partially wetting fluid. *Phys. Rev. Lett.* **89**, 244501 (2002).
23. Huang, Y. G. Y. *et al.* Stamp collapse in soft lithography. *Langmuir* **21**, 8058–8068 (2005).
24. Hui, C. Y., Jagota, A., Lin, Y. Y. & Kramer, E. J. Constraints on microcontact printing imposed by stamp deformation. *Langmuir* **18**, 1394–1407 (2002).
25. Zhu, X. Y. *et al.* Fabrication of reconfigurable protein matrices by cracking. *Nature Mater.* **4**, 403–406 (2005).
26. Bowden, N., Huck, W. T. S., Paul, K. E. & Whitesides, G. M. The controlled formation of ordered, sinusoidal structures by plasma oxidation of an elastomeric polymer. *Appl. Phys. Lett.* **75**, 2557–2559 (1999).
27. Schmid, H. & Michel, B. Siloxane polymers for high-resolution, high-accuracy soft lithography. *Macromolecules* **33**, 3042–3049 (2000).
28. Odom, T. W., Love, J. C., Wolfe, D. B., Paul, K. E. & Whitesides, G. M. Improved pattern transfer in soft lithography using composite stamps. *Langmuir* **18**, 5314–5320 (2002).
29. Decre, M. M. J., Timmermans, P. H. M., Sluis, O. & Schroeders, R. Numerical and experimental study of critical roof collapse conditions in soft lithography. *Langmuir* **21**, 7971–7978 (2005).
30. Beebe, D. J. *et al.* Functional hydrogel structures for autonomous flow control inside microfluidic channels. *Nature* **404**, 588–590 (2000).

Acknowledgements

We thank M. Mayer for comments on the manuscript, N. Futai for assistance in electrical resistance measurements, J. H. Bahng for help with channel fabrication and K. E. Sung for preparing DNA samples. We thank K. Naruse for the mechanical stretcher device. This work was supported by NSF, NIH and the NASA BioScience and Engineering Institute. D.H. acknowledges a Horace H. Rackham Predoctoral Fellowship from the University of Michigan.
Correspondence and requests for materials should be addressed to S.T.
Supplementary Information accompanies this paper on www.nature.com/naturematerials.

Author contributions

D.H. designed and fabricated the nanochannel systems, carried out the experiments, analysed the data and wrote the manuscript. K.L.M. conducted numerical simulations of nanochannel closure and helped to write the paragraphs describing the simulation results. X.Y.Z. helped to take AFM measurements of nanochannel cross-sections. M.A.B. helped to plan DNA stretching experiments and provided DNA samples. M.D.T. helped to design the simulation studies, interpreted simulation results and edited the manuscript. S.T. designed the project and edited the manuscript. All authors commented on the manuscript.

Competing financial interests

The authors declare no competing financial interests.